OPTOELECTRONICS AND ADVANCED MATERIALS – RAPID COMMUNICATIONS Vol. 4, No. 5, May 2010, p. 671 - 680

Relaxor behavior of $(Na_{0.5}\ Bi_{0.5})\ TiO_3$ Ceramic with simultaneous substitution of Ba^{2+} and Zr^{4+}

K. SAMBASIVA RAO*, B. TILAK, K. CH. VARADA RAJULU, P. MURALI KRISHNA
Department of Physics, Andhra University, Visakhapatnam-530003, India

$0.94(Bi_{0.5}Na_{0.5})Ba_{0.06}Z_{0.04}T_{0.96}O_3$ (0.06BNBZT) ceramic has been prepared by conventional solid state reaction method. Effect of simultaneous substitution of Ba^{2+} (A-site) and Zr^{4+} (B-site) in $Na_{0.5}Bi_{0.5}TiO_3$ (NBT) on structure, dielectric, impedance and conductivity (35-600^{0}C & 45Hz -5MHz) have been studied. X-ray diffraction studies indicated a rhombohedral structure. Crystallite size, strain analysis has been done by Debye - Scherrer and Williamson-Hall technique. The tolerance factor of 0.81 indicated the stable Perovskite structure of the material. Relaxor type behaviour is reveled by diffuse phase transition (γ = 1.45) and the frequency dependence of T_m has been modeled through Vogel-Fulcher relation. Impedance analysis showed the non-Debye type relaxation. Conductivity in the material followed the Jonscher's law, $\sigma = \sigma_0 + A\omega^n$. The theoretical values of ε^1 computed using the 'A(T)' and 'n(T)' ($0<n<1$) parameters are well fitted with experimental curves. The activation energies from different formalism confirmed the ionic type conduction in material the influence of and oxygen vacancies.

(Received March 01, 2010; accepted May 20, 2010)

Keywords: (Na, Ni) TiO_3, Ceramic, Relaxor

1. Introduction

Disordered oxide ferroelectrics with perovskite type ABO_3 structure have been receiving a considerable attention due to their promising dielectric relaxor, semiconducting, Pyroelectric and electromechanical, properties. Smolenskii.et.al [1950] initially reported the relaxor behaviour in ferroelectric Ba(Ti Sn)O_3 solid solution [1]**.** But, today's most of the consumer electronic products are manufacturing with lead based compounds, e.g. PbTiO3, $Pb(Mg_{1/3}Nb_{2/3})O_3$,etc,[2-4]. But, the environmental organizations suggesting for prohibit these materials due to hazardous nature of lead. Hence, the search for lead free materials for consumer electronics, MLCC, transducers, etc, applications has become a central idea of the present day materials research [5].

The Sodium bismuth titanate (NBT)- based ceramics are good alternative to the present dominating PMN-PZT compounds, and the existence of large ferroelectricity may be due to $(Bi_{1/2}Na_{1/2})^{2+}$ ions in A- sites of the perovskite structure. It is also reported that the NBT has been exhibiting a relaxor type diffuse phase transition [6-8]. Further, the titanium based materials are interesting as they are suitable for room temperature applications. The selection of dopants to tailor the physical properties of these materials is based on many factors including (i) charge neutrality (ii) tolerance factor (t) (iii) the ionic radius (iv) solubility/miscibility [9]. Several literature reports were made on electrical properties of the solid solution of NBT modified (either A or B-sites) with various perovskite like $BaTiO_3$ [10-14] $SrTiO_3$ [12,15-17], $PbTiO_3$[18,19], $CaTiO_3$ [20] $(K_{0.5}Bi_{0.5})TiO_3$ [19,21,22], $(K_{0.5}Bi_{0.5})TiO_3$- $BaTiO_3$ [23,24], $(Na_{0.5}Bi_{0.5})(Zr_{0.25}Ti_{0.75})O_3$ [25], etc.

Different physical models were proposed to explain the diffuse phase transition in relaxor ferroelectrics [8,26-29]**.** From physical point of view, the diffuse phase transition is generally attributed to the randomly oriented polar micro-regions originated from compositional fluctuations on the nanometer length scale [26]. L.E Cross et.al [8] extended the smolenskii's model to a super-paraelectric model. In this model, the sizes of nano polar regions are characterized by the spatial coherence of their spontaneous polarization. Each nanopolar region was considered as the source of dipolar entity with no interaction among each other. The relaxor behaviour was attributed to these nanometer size regions to a thermally activated ensemble of super-paraelectric clusters. The broad distribution of the relaxation times for cluster orientation originates from the distribution of the potential barriers separating the different orientational states.

The single crystals of $(Bi_{1/2}Na_{1/2})_{1-x}Ba_xTiO_3$ (BNBT) grown by cation nonstichiometry showed a high d_{33} value of 650pC/N and K_t upto 0.57 in rhombohedral phase [30-33]. When the same is modified with Zr^{4+} (i.e., BNBZT, rhombohedral phase) attained a further higher value,d_{33}=1180 pC/N, which has been estimated directly from the slope of strain Vs electric field measurements [34]. Complex impedance spectroscopy is a convenient tool to analyze the contribution of electrical components such as grain (R_g) (bulk), grain–boundary (R_{gb}) or polarization phenomena. These parameters have pronounced influence the device properties of materials. Using the Cole-Cole plots, one can measure the R_g ,R_{gb} values and is represented by equivalent parallel RC circuit.

Our extensive literature survey indicated that no attempt has been made so far to characterize the electrical properties $0.94(Bi_{0.5}Na_{0.5})Ba_{0.06}Zr_{0.04}Ti_{0.96}O_3$ (0.06BNBZT) ceramic using dielectric spectroscopy technique. In view

of the excellent properties exhibited by the material, the present communication illustrates the synthesis, structure, dielectric (ε), impedance (Z) and conductivity (σ) properties of 0.06BNBZT studied by dielectric spectroscopy technique.

2. Compound synthesis

Polycrystalline $0.94(Bi_{0.5}Na_{0.5})Ba_{0.06}Zr_{0.04}Ti_{0.96}O_3$ (0.06BNBZT) ceramic has been synthesized by solid state reaction method. Initially, AR grade chemicals $BaCO_3$, Na_2CO_3, Bi_2O_3, ZrO_2 and TiO_2 were taken in stochiometric ratios. After vigorous grounding in agate mortar and pestle, the mixture has been calcined at 850^0C for 3 hrs. The grinding and calcination procedure has been repeated for two times to achieve homogenous, single phase powder which is confirmed via X-ray powder diffraction (XRD) technique. The loss of the oxides and carbonates has been verified before and after the calcination. Required amount of PVA (poly vinyl alcohol) organic binder has been added and thoroughly mixed. This provides the strength, flow ability of granules and to reduce the brittleness of the sample. Then, the granulated powder is compacted into discs of 11mm diameter and 3 mm thickness using a hydraulic press under 700Mpa pressure and the pellets are placed on a platinum foil to sinter at different temperature and stay times (1150^0C-1200^0C/3hrs). The sample sintered at 1180^0C/3hrs attained a higher density upto 98% of theoretical density.

3. Experimental

Room temperature powder diffraction analysis has been performed using Philips X-ray diffractrometer with CuKα radiation (λ=1.5406A^o). The lattice parameters of unit cell (a,b,c) and indexing (hkl) for peaks were done by computer program package- interpretation and indexing program by E.Wu. School of physical science,Flinders University, South Australia. The microstructure on the specimens of present investigation were obtained with scanning electron microscope (SEM) (JEOL_JY :Model 5800F).The measurement of permittivity, impedance, and conductivity has been carried out by computer interfaced LCR Hi-tester 3532-50, HIOKI corporation, Japan over wide range of temperature (35 - 600^0C) and frequency (45Hz-5MHz). Silver electrodes were deposited on the circular faces of the sample before performing the investigation.

4. Results and discussion

4.1 Structure

The X-ray diffraction pattern of 0.06BNBZT is shown in Fig.1. The maximum intensity peak of the material is observed at $2\theta = 32.4^0$. The lattice parameters computed are a=b=c=3.87Å with index set (110) revealing the material belongs to rhombohedral structure with small distortion [35]. These values are in agreement with the values as reported [36].

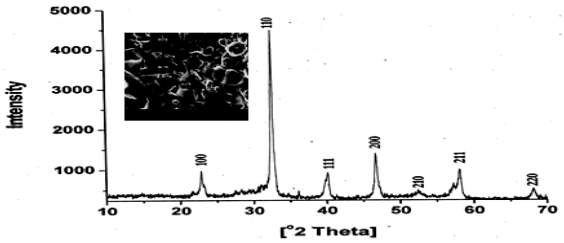

Fig. 1. XRD pattern of 0.06BNBZT.

The theoretical density (ρ_{cal}) of the sample is calculated using the formula,

$$\rho = \frac{cell\ mass}{cell\ volume} = \frac{n \times M \times 1.66 \times 10^{-24}}{V} g/cm^3 \qquad (1)$$

where n is the number of atoms per unit cell, M is the molecular weight of atoms constituting one unit of the chemical formula, and V is the unit cell volume [**37].** The experimental density (ρ_{cal}) is calculated using Archimedes principle. The values of lattice parameters, density, and porosity of the material have been given in Table 1. The insert of the Fig 1 show the SEM micrograph of polished surfaces of the sintered pellet of 0.06BNBZT. The grain size of the sample has been calculated from linear intercept method. The observed average grain size from micrograph is 1.51 μm.

Table 1. Lattice parameters and Density 0.06BNBZT.

Sample	Lattice parameters (Å)	Cell Volume (Å^3)	Density(gm/cm^3) ρ_{cal}	ρ_{Exp}	%	Porosity
0.06BNBZT	a=3.87	58.32	6.11	5.99	98	0.02

4.1.1 Crystallite size and strain analysis

(a) Debye-Scherrer analysis

One can say that no crystal is perfect due to its limited size. Such a deviation from perfect crystallinity will lead to broadening of the diffraction peak.

However, this type of peak broadening is negligible when crystallite size is larger than 200nm. Crystallite size is a measure of coherently diffraction domain. Scherrer first observed that small crystallite size could give rise to

peak broadening. The average crystallite size has been calculated by the formula,

$$t = \frac{K\lambda}{\text{Bcos}\ \theta}$$

where, t is the averaged dimension of crystallite, the Scherrer constant (K=0.89), λ is the wavelength of X-ray (λ=1.5406Å), β or B= full width half maxima (FWHM) of broadening diffraction line on the 2θ scale(radians). The estimated values are given in Table 2.

(b) Williamson-Hall technique

Williamson-Hall [38] expressed integral breadth (β) for all reflections of the sample in terms of reciprocal unit β* (β*= β cos(θ)/λ) as a function of d*(d*=2 sin(θ)/λ) as fallows,

$$\frac{\text{Bcos}\ \theta}{\lambda} = \frac{1}{\text{D}} + 2\varepsilon[\frac{2\ \sin(\theta)}{\lambda}]$$

where, β(orB) is the difference in integral breath between a standard (β_{std}) and experimental (β_{obs}), D the average crystallite size, λ is wave length of X-ray diffraction pattern and ε is the average micro strain.

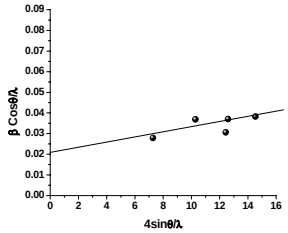

Fig. 2. Williamson-Hall plot of 0.06BNBZT.

The slope of the plot (Fig. 2) drawn for B cos θ/λ as a function of 4 sin(θ)/λ gives the value of micro strain and intercept results crystallite size. The average Crystallite size and micro strain of the 0.06BNBZT has been estimated by using the Willamson-Hall plot approach. The calculated values of micro strain and crystallite size are given in Table 2. In Williamson-Hall method the strain component neglected, hence the crystalline size is larger compared to Debye-Scherrer method.

Table 2. Crystallite size by Debye -Scherrer and Williamson-Hall.

Sample	Average Crystallite size (nm) Debye Scherrer technique	Average Crystallite size (nm) William son Hall Technique	Average microstrain ε (x 10^{-3})
0.06BNBZT	32	48	1.20

4.1.2 Tolerance factor

The tolerance factor (t) is determined by the formula ,

$$t = \frac{(r_A + r_o)}{\sqrt{2}(r_B + r_o)}$$

where r_A, r_B and r_o are ionic radii of A-site cation (Ba^{2+}=1.34Å, Na^{+1}=0.97Å,Bi^{+3}=0.96Å), B-site cations (Zr^{+4}=0.79 Å, Ti^{+4}=0.68 Å) and anion (O^{2-}=1.32 Å) respectively. By substituting the ionic radii of the material 0.06BNBZT, the tolerance factor t=0.81 is estimated, which is in the limit of stable perovskite structure **[39].** Generally, the value of t<1 suggests an anti ferroelectric property. The present material shows ferroelectric property due to the considerable energy of electrostatic dipole-dipole interactions. This is explained by a sufficiently large dipole moment of A site ions and reduction in the difference between the moment of the A and B (Ti^{4+}) ions which favors the ferroelectric state. The presence of Bi^{3+} ions increases the degree of covalency of chemical bonds, electronic polarizability of oxygen ions results the relative stability in ferroelectric and anti-ferroelectric state [40].

4.2 Electrical properties

4.2.1 Dielectric studies

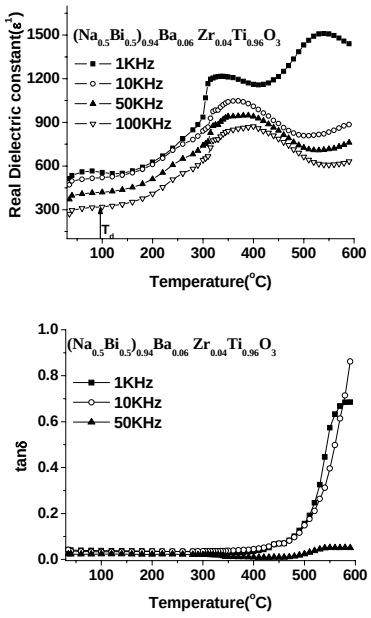

Fig. 3. Temperature dependence of dielectric constant and dielectric loss of 0.06BNBZTat different frequencies.

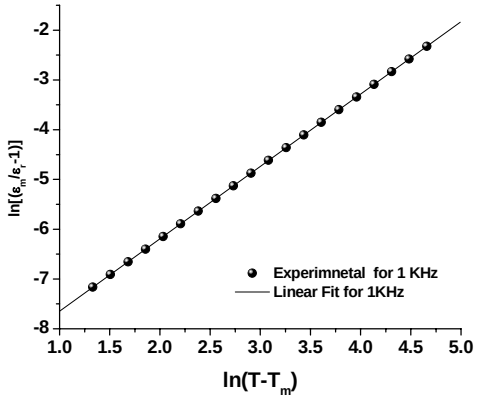

Fig. 4. Variation of ln[(εm/ εr)-1] against ln(T-Tm) 0.06BNBZT at 1 KHz.

Fig. 3 shows the temperature dependence of the real dielectric constant (ε^1) in 0.06BNBZT. The value of ε^1 increases gradually to a maximum value (ε_m) with increase in temperature and then decreases after phase transition. From the plots, a broad peak (diffuse), with a decrease of magnitude with increase in frequency has been observed. Further, the maximum shift towards higher temperature region, indicating the dielectric polarization is of relaxation type in 0.06BNBZT material. The dielectric anomaly and frequency dispersion may be due to slowing down of superparaelectric moments [5]. In relaxor ferroelectrics, the dielectric permittivity near the Curie region is governed by the modified Curie-Weiss law. Martirena and Burfoot [41] proposed a power relation to describe the temperature dependence of the relative dielectric permittivity in the paraelectric phase as

$$\frac{1}{\varepsilon_r(\omega,T)} = \frac{1}{\varepsilon_m(\omega)} 1 + \left[\frac{[T - T_m(\omega)]^\gamma}{2\delta_\gamma^2}\right] \qquad (2)$$

where, ω is the angular frequency, T_m is the temperature at maximum dielectric permittivity ε_m,; δ_γ , γ are the diffuseness parameter and critical exponent respectively. The parameter γ ($1 \le \gamma \le 2$) represents the degree of dielectric relaxation of a relaxor. The value of $\gamma \le 1$ indicates Curie-Wiess behaviour of the ferroelectric, while $\gamma \le 2$ is identical to a quadratic Smolensky's relation [42]. From the extended Curie-Wiess law (Eq.2), the slope of the plot of $\ln[(\varepsilon_m/\varepsilon_r)-1]$ against $\ln(T-T_m)$ provides the value of γ. The plot obtained from Eq.2 at 1KHz is shown in Fig. 4. The evaluated the value of γ (Table 3) suggesting the diffuse phase transition is due to the microscopic heterogeneity in the compound with different local Curie points. This is in agreement with the reported result [43].

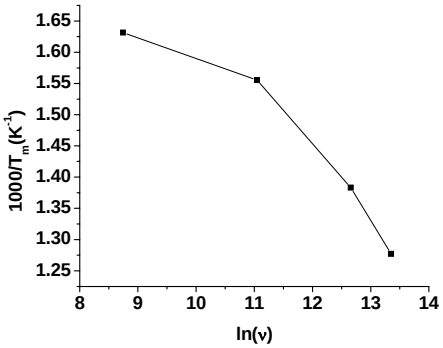

Fig. 5. Plot of ln(ν) against 1/Tm of 0.06BNBZT.

The variation of dielectric constant and non-polar space group suggests that the material may have ferroelectric phase transition. The variation of inverse of temperature with angular frequency taken on log scale i.e. ln(ν)Hz has been show in Fig. 5. The nonlinear nature observed in the Figure confirming that, a simple Debye equation cannot be fitted to the sample. Therefore, the relaxation times can be expressed by the Vogel- Fulcher law [44,45]. In order to analyze the relaxation features, i.e., relation between ν and T_m of the ceramic, the experimental curves were fitted using the Vogel Fulcher formula[46,47].

$$\nu = \nu_0 \exp\left[\frac{-E_a}{K_B(T_m - T_f}\right]$$

where, ν_0 is the attempt frequency, E_a the measure of average activation energy, K_B the Bolzmann constant, and T_f is the temperature at which dynamic reorientation of the dipolar cluster polarization can no longer be thermally activated.

The Vogel- Fulcher relationship may be interpreted as a normal Debye relaxation with temperature-dependent activation energy. The activation energy increase as the temperature decreases. The more realistic interpretation of this relationship in reference to relaxors is that E_a represents the activation energy for polarization fluctuations of an isolated cluster with temperature dependence arising from the development of short –range order between neighbor clusters with K_BT_f being a measure of the interaction energy. The ferroelectric clusters interaction may take place via dipole and dipole-dipole induced exchanges. The possibility also exists in elastic interaction of clusters could through local rhombohedral distortion. This also implies that the clusters may freeze into orientation glassy state and are superparaeleastic above the freezing temperature.

Table 3. Dielectric parameters of 0.06BNBZT (at 1 KHz).

Sample	T_m (°C)	ε_m	Γ
0.06BNBZT	340	1216	1.47

The slope of the line in fitted (Fig. 5) resulted the activation energy E_a=0.0140eV. This reveals the relaxor behaviour in 0.06BNBZT system. The relaxor behaviour in PMZT-PT, $Ba_{1-x}Bi_{2x/3}Ti_{0.75}Zr_{0.25}O_3$ has been also reported [48, 49]**.** In the present ceramic, the relaxor behaviour has been ascribed to microscopic composition fluctuations, the merging of micropolar regions into macropolar regions, or a coupling of order parameter and local disorder mode through the local strain.

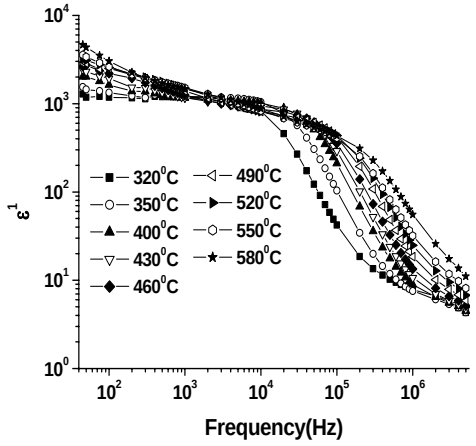

(a)

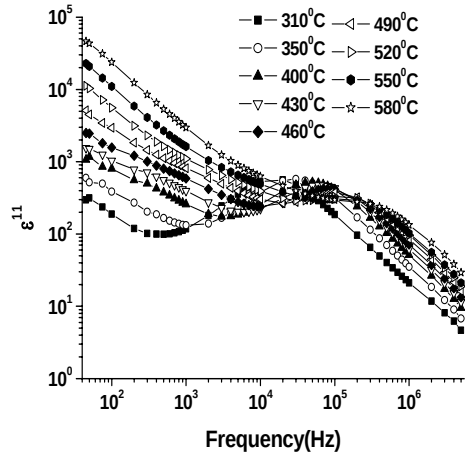

(b)

Fig. 6. Frequency dependence of (a) real ε^1 ,(b)Imaginary ε^{11} parts of the dielectric constant at several temperatures on 0.06BNBZT.

Fig. 6 (a) and (b) represents the frequency dependence of the real (ε^1) and imaginary (ε^{11}) part of dielectric constant at different temperatures in 0.06BNBZT. Both ε^1, ε^{11} showed a strong dispersion at low frequencies and is strongly affected by the change in temperature. Such a strong dispersion in dielectric constant is a common feature in the ferroelectrics associated with good ionic conductivity and is referred to as low frequency dielectric dispersion, [LFDD] [50, 51]. Jonscher and Hill [52, 53] have dealt with LFDD phenomena in detail. The dispersion in the imaginary part of the dielectric constant (**ε^{11}**) is stronger than that of the real part (**ε^1**) (Fig. 6(b)). The low frequency slope of the curve of ε^{11} is close to -1 indicating the predominance of dc conduction in this frequency region. In the high frequency region the slope lies between 0 and -1, depending on the temperature.

According to Jonscher's universal law, the complex dielectric constant, $\varepsilon^*(\omega)$ can be expressed as,

$$\varepsilon^* = \varepsilon' - i\varepsilon'' = \varepsilon_\infty + \frac{\sigma}{i\varepsilon_o\omega} + \frac{a(T)}{\varepsilon_o}(i\omega^{n(T)-1}) \qquad (3)$$

where ε_∞ is the 'high frequency' value of dielectric constant, n(T) the temperature dependent exponent, which determines the strength of the ion –ion coupling (smaller value of n(T) corresponds to strongly interacting systems) and a(T) determines the strength of the polarizibility arising from the universal mechanism. The real and imaginary parts of the dielectric constant from Eq.3 are given by,

$$\varepsilon^1 = \varepsilon_\infty + \sin(n(T)\pi/2)\ (a(T)/\varepsilon_0)\ (\omega^{n(T)-1}) \qquad (4)$$

$$\varepsilon^{11} = \sigma/\varepsilon_0\,\omega + \cos(n(T)\pi/2)\ (a(T)/\varepsilon_0)\ (\omega^{n(T)-1}) \qquad (5)$$

where, the first term in Eq. 4 characterizes the lattice response and that in Eq.5 reflects the dc conductiion part, while the second term in both the equations refers to the charge carrier contributions to the observed dielectric constant. Dielectric relaxation in perovskite ferroelectrics represents the change in polarization according to a time variant electric field. In general, the dielectric properties are strongly influenced by the complexity of grain boundaries,grain size and orientation, and ionic space charge carriers. For a constant value of n, Eq.3 represents a straight line with a slope equal to (n-1) in the logarithmic plot of ε^1 and frequency. The 'exponent-n(T)' describes the interaction between the charge carriers that are participating in the polarization [54]. In Debye case, n=1 and $n \leq 1$ for non-Debye type, having a translation motion with sudden hopping. The value of n >1, indicates a localized hopping.

In 0.06BNBZT, the value of n (Fig. 7(a)) decreases with increase in temperature suggesting a strong uncorrelated reorientation of the charge carrier polarization at T_m. In vicinity of the transition temperature, the dielectric constant strongly influenced by the polarization due to the carriers and strong low frequency dielectric dispersion is found over a wide temperature range [55]**.** The pre-factor A(T), which is temperature dependent (Fig.7(b)), determines the strength of the polarizability. In the studied material, the pre-factor value increases with increase in temperature upto T_c at 1KHz with a subsequent decrease. The higher value of A at T_c may be due to longer relaxation time.

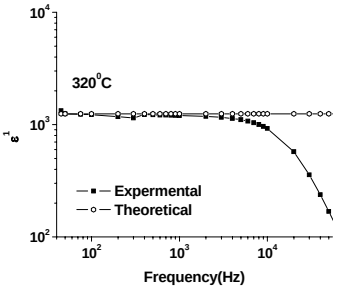

Fig. 8. Fitting results for dielectric constant of 0.06BNBZTat 320^{0}C.

The theoritical values of ε^1 are estimated by putting the values of n(T) and A(T) in Eq.4, and are fitted with the experimental data at 320^{0}C typically as shown in Fig. 8. The plot shows a good agreement between experimental and theoretical values of ε^1 at higher frequencies.

4.2.2 Impedance studies

Fig. 9 (a) shows the variation of the real part of the impedance (Z^1) with frequency at various temperatures. It is observed that the magnitude of Z^1 decreases with the increase of frequency and temperature, indicating an increase in AC conductivity. The merging of Z^1 curves at all temperatures above 10 KHz is ascribed to the release of space charges as a result of reduction in the barrier properties. This may be involved in the enhancement of AC conductivity of material with temperature at higher frequencies.

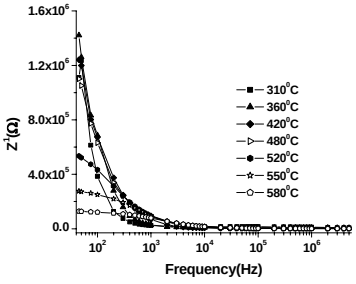

(a)

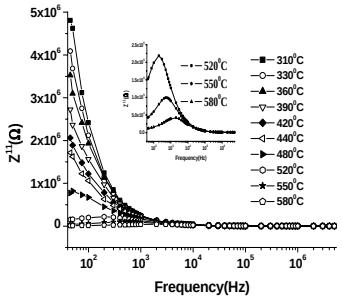

(b)

Fig. 9.Variation of (a) real Z^1 and (b) Imaginary (Z^{11}) parts of Impedance with frequency at different temperature in 0.06BNBZT.

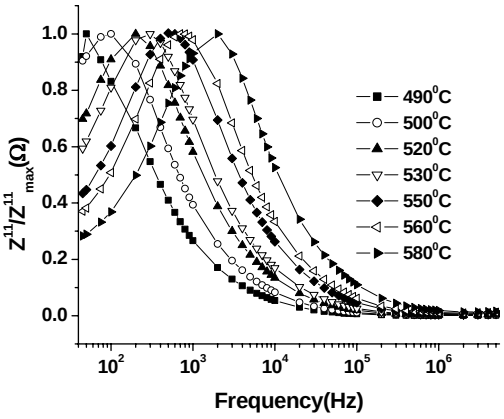

(a)

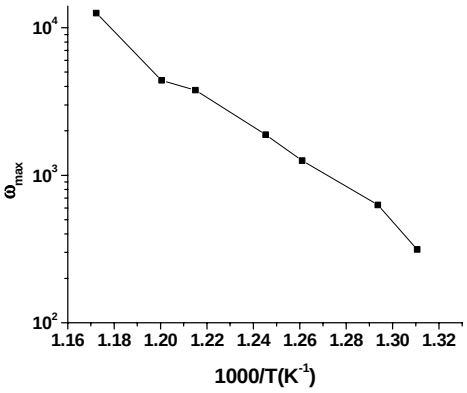

(b)

Fig. 10. (a) Normalized imaginary parts Z^{11}/Z^{11}_{max} of impedance as a function of frequency .(b) Temperature dependence of relaxation frequency for 0.06BNBZT.

Fig. 9 (b) shows the variation of imaginary part of impedance Z^{11} with frequency at different temperatures. The curves show that the Z^{11} value reaches a maxima peak (Z^{11}_{max}) above 300^{0}C and the peak shifts to higher frequencies side with increasing temperature, revealing the spread of relaxation times. Therefore, the temperature dependent electrical relaxation phenomenon exists in the material [56]. The merge of Z^{11} values in the high frequency region is an indication of the accumulation of space charge in the material.

The normalized imaginary part (Z^{11}/Z^{11}_{max}) of impedance as a function of frequency at several temperatures in 0.06BNBZT has been shown in Fig.10a. The Z^{11}/Z^{11}_{max} parameter exhibited a peak of slightly asymmetric degree at each temperature indicating the triggering of another relaxation process. At the peak, the relaxation is defined by the condition $\omega_m\tau_m=1$, where, τ_m is relaxation time at the peak. The relaxation frequency obeys the Arrhenius relation given by $\omega_m= \omega_o\exp[-Er/K_BT]$, where, ω_o is pre exponential factor, and the activation energy (Fig.10b) is found to be Ea=0.89eV.

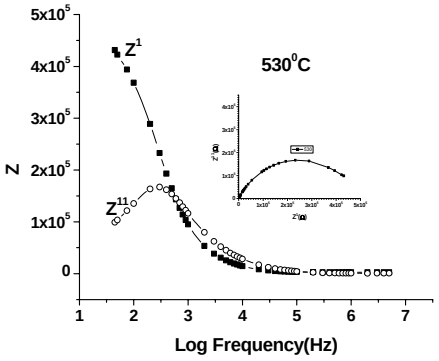

Fig. 11. Frequency dependence of Z^1 and Z^{11} ; (Insert) Corresponding Argand diagram of 0.06BNBZT.

Fig. 11 shows the frequency dependence of Z^1 and Z^{11} at different temperatures and Argand diagram typically drawn at 530^0C [57,58]. These plots are indicating the existence of impedance relaxation phenomena. Complex impedance formalism provides information about the relaxation process and gives frequency dependent phenomena associated with grain boundaries region and intrinsic properties of the material in the system. Cole-Cole plots [59] (Z^{11}vs Z^1) of 0.06BNBZT at different temperatures (430^0C-550^0C) has been shown in Fig. 12 (a).

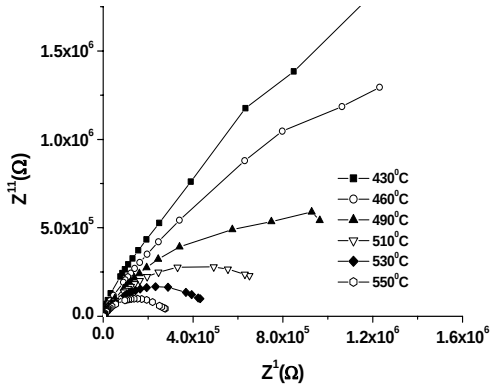

(a)

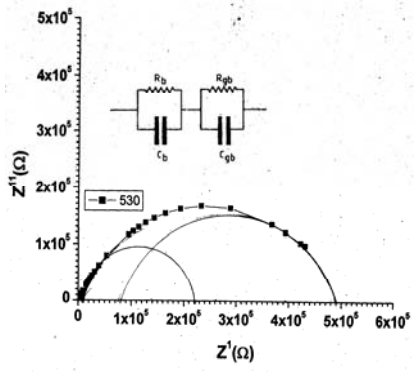

(b)

Fig. 12. (a)Cole -Cole Plots for 0.06BNBZT, (b) At different temperature equivalent circuit.

As shown in Fig. 12 (a), a straight-line response has been observed below 430^0C. As the temperature increases, a turn into semi-circles observed with a decrease in size has been observed. This trend indicates the reduction of grain (Rg), grain boundary (Rgb) resistance and negative temperatures coefficient of resistance (NTCR) behaviour like semi conducting materials [60-62]. At higher temperatures, the Cole-Cole plots are resolved into two overlapping arcs suggests the contribution of two relaxation mechanisms due to grain and grain boundary. The centre of semi circles lies below the x-axis at an angle 'ø' indicating non-Debye type relaxation process in 0.06BNBZT. The observed data indicating that the conduction in 0.06BNBZT is predominant through grain boundary and giving a scope for variety of device applications.

4.2.3 Conductivity studies

Fig. 13 (a) shows the electrical conductivity σ(ω) as a function of frequency at different temperatures in 0.06BNBZT. The trend representing that conductivity in the ceramics is following the Jonscher law [52], $\sigma(\omega) = \sigma_{dc} + A\omega^n$, where σ_{dc} is frequency independent conductivity, the coefficient A and the frequency exponent n are thermally activated material dependent quantities. The term $A\omega^n$ contains ac dependence and characterizes all dispersion phenomena.

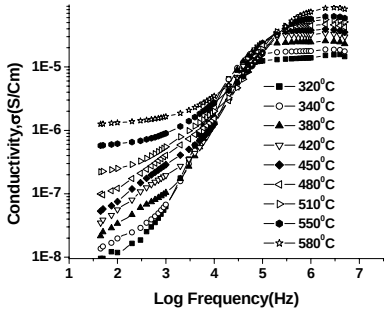

(a)

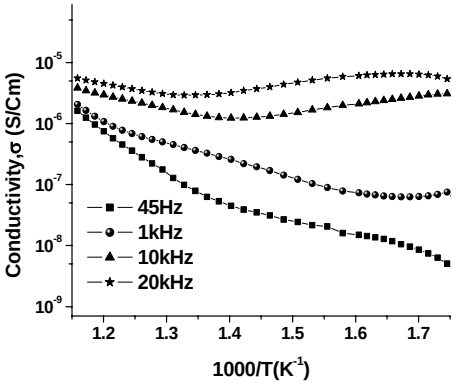

(b)

Fig. 13. (a) Frequency dependence of real part of AC conductivity at various temperatures (b) Variation of AC conductivity as function of inverse of temperature.

In the present material, the ac conductivity is found to increase with increase in frequency suggesting the bound carriers trapped in the sample. The slowly varying conductivity at lower frequencies corresponds to space charge polarization [63]. Also, a change in slope has been observed at a particular frequency is related to ion hopping frequency [64-66].

The conductivity is found to obey the Arrhenius behaviour. Fig.13 (b) shows the variation of conductivity (σ_{dc} and σ_{ac}) with inverse of temperature at different frequencies in 0.06BNBZT material. In low temperature region (298^0C -398^0C), the conductivity showed dispersion, while, curves are merged at high temperatures region, revealing predominance of an onset of intrinsic conductivity mechanism. The activation energies of ac and dc conductivity in the materials have been evaluated and are given in Table 4.

Table 4. DC and AC conductivity activation energies of 0.06BNBZT.

Temperature (^{O}C)	Conductivity Activation Energy (eV)			
		AC		
	DC	1KHz	10KHz	20KHz
310-350	0.60	0.09	0.11	0.08
360-400	0.21	0.45	0.13	0.01
410-460	0.30	0.22	0.19	0.03

From the calculated values, the activation energy for dc conductivity is found to be more than the ac conductivity. This may be due to hopping of charge carriers in the considered temperature region. The ac conductivity activation energies are increased with increase in temperature. The low values of activation energies may be due to the carrier transport through hopping between localized states in disordered manner. The conduction at higher temperatures might be due to oxygen vacancies and the conductivity in 0.06BNBZT is thermally activated.

The temperature dependence of the dc conductivity and the hopping frequency follows the Arrhenius behaviour expressed by the Eq.6 and Eq.7.

$$\sigma_{dc} = \sigma_0 \exp\left(\frac{-U_{dc}}{K_B T}\right) \quad (6)$$

$$\omega_H = \omega_0 \exp\left(\frac{-U_H}{K_B T}\right) \quad (7)$$

where, U_{dc} ,U_H are the activation energies of the dc conductivity and the hopping frequencies of the carriers respectively, σ_o ,ω_o are pre-exponential factors.

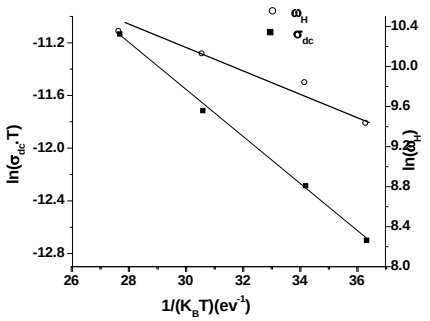

Fig. 14. Arrhenius dependence of dc conductivity (σ_{dc}) and the hopping frequency (ω_H).

The activation energies (Fig. 14) of U_{dc} and U_H are estimated to be 0.17 eV, 0.12eV respectively.

The value of activation energies again allowed us to confirm the oxygen vacancies are dominant charge carrier in 0.06BNBZT. Further, it is expected that spontaneous polarization originating from the off of center displacement of Ti^{4+} ions from the anionic charge center of the oxygen octahedron for the ceramic phase [67, 68] which dominates the dielectric response of the material [69]. The presence of oxygen vacancies would distort the actual ionic dipoles due to the Ti^{4+} ions. The decay of polarizations due to distorted ionic dipoles could be the cause for the dielectric relaxation process. Thus, the relaxation process for the studied material (0.06BNBZT) is attributed to the decay of polarization in the oxygen defect-related dipoles due to their hopping conduction.

5. Conclusions

Ceramics of $0.94(Bi_{0.5}Na_{0.5})Ba_{0.06}Zr_{0.04}Ti_{0.96}O_3$ (0.06BNBZT) synthesized by conventional solid-state reaction route exhibited rhombohedral structure at room temperature. The diffused phase transition confirmed the relaxor type ferroelectric and is explained in terms of formation of nanopolar regions. The extended Curie-Wiess law resulted the diffusiveness parameter, γ= 1.45, the activation energy, Eg= 0.28eV is found by Vogel-Fulcher relation. Cole-Cole plots showed the non-Debye type relaxation in the material with predominant grain-boundary conduction. The anomalies observed at T_m in the exponential parameter n(T) and pre-factor A(T), suggesting uncorrelated reorientation of the charge carrier polarization and strength of the polarizability in 0.06BNBZT. The activation energies U_{dc} =0.17 eV and U_H =0.12eV confirmed the oxygen vacancies conduction mechanism is dominant in higher temperature region.

Acknowledgements

The authors K.S.Rao and K.Ch.Varadarajulu thanks to Naval Science and Technology Laboratory (NSTL), Govt of India, Visakhapatnam, for funding the research project.

References

[1] G. A. Smolenskii, V. A. Isopov, Dokl. AKad, nauk SSSR **9**, 653 (1954).
[2] G. A. Smolenskii, A. I. Agranovskaya, Soc.Phys. Tech. Phys. **3**, 1380 (1958).
[3] N. Setter, R. Waser, Acta Matter **48,** 151 (2000).
[4] Y. Yamoshita, Am. Cera. Soc. Bull **73,** 74 (1994).
[5] S. B. Krupanidhi, Proc. Indian Acad. Sci.(Chem.sci) **115**(5-6), 775 (2003).
[6] G. A. Smolenskii, V. A. Isopov, I. Agransovskaya, N. N. Krainik, Sov. Phys. Solid State **2**, 2651 (1961).
[7] S. G. Lungshnikov, S. N. Gvasaliya, I. G. Siny, I. L. Sashin, V. H. Schmidt, Y. Useu, Solid state Comm. **116**, 41 (2000).
[8] L. E. Cross, Ferroelectric **76,** 241 (1987).
[9] S. Sen, P. Pramanik, R. N. P Choudary, Appl. Phys. A. **82**, 549 (2006).
[10] Y. Hosono, K. Harada, Y. Yamashita, Jpn. J. Appl. Phys. **40,** 5722 (2001).
[11] J. Suchanicz, J. Kusz, H. Bhöm, H. Duda, J. P. Mercurio, K. Konieczny, J. Eur. Ceram. Soc **23**, 1559 (2003).
[12] J. R. Gomah Pettry, S. Said, P. Marchet, J. P. Mercurio, J. Eur. Ceram. Soc. **24,** 1165 (2004).
[13] Q. Xu, S. Chen, W. Chen, S. Wu, J. Zhou, H. Sun, Y. Li, Mater. Chem. Phys. **90,** 111 (2005).
[14] R. Ranjan, A. Dviwedi, Solid State Commun. **135,** 394 (2005).
[15] J. R. Gomah-Pettry, A. N. Salak, P. Marchet, V. M. Ferreira, J. P. Mercurio, Phys. Status Solidi (b) **241,** 1949 (2004).
[16] S. E. Park, K. S. Hong, J. Mater. Res. **129,** 279 (1997).
[17] J. K. Lee, K. S. Hong, C. K. Kim, S. E. Park, J. Appl. Phys. **91,** 4538 (2002).
[18] S. Said, P. Marchet, T. Merle, Mejean, J. P. Mercurio, Mater. Lett. **58,** 1405 (2004).
[19] S. Said, J. P. Mercurio, J. Eur. Ceram. Soc. **21,** 1333 (2000).
[20] B. V. B. Saradhi, K. Srinivas, T. Bhimasankaram, Int. J. Mod. Phy. B **16**, 1 (2002).
[21] Y. Li, W. Chen, J. Zhou, Q. Xu, H. Sun, M. Liao, Ceram. Int. **31,** 139 (2005).
[22] J. Yoo, D. Oh, Y. Jeong, J. Hong, M. Jung, Mater. Lett. **58,** 3831 (2004).
[23] Y. Li, W. Chen, Q. Xu, J. Zhou, X. Gu, S. Fang, Mater. Chem. Phys. **94,** 328 (2005).
[24] Y. M. Li, W. Chen, Q. Xu, J. Zhou, X.. Gu, Mater. Lett. **59,** 1361 (2005).
[25] Lily, K. Kumari, K. Prasad, R. N. P. Choudhary, Journal of alloys and Compounds **453,** 325 (2008).
[26] G. A. Smolenskii, Sov. Phys. Solid State **6**, 1676 (1965).
[27] D. Viehland, S. Jang , L. E. Cross, M. Wutting, J. Appl. Phys. **68**, 2916 (1990).
[28] V. A. Bokov, I. E. Myl'nikova, Sov. Phys. Solid state **3**, 613 (1961).
[29] V. Westpha, W. Kleeman, M. D. Glinchuk, Phys. Rev. Lett. **68,** 847 (1992).
[30] Y. M. Chiang, G. W. Farrey, A. N. Soukhojak, Appl. Phys. Lett. **73**, 3683 (1998).
[31] G. W. Farrey, A. N. Soukhojak, S. Sheets, Y. M. Chiang, IEEE International symposium on Application of ferroelectric, Montreux, Switzerland, 1998 (IEEE, Newyork,1991), 551.
[32] Y. M. Chiang, G. W. Farrey, A. N. Soukhojak, S. A. Sheets, Proceedings of the ninth US-japan Seminar on Dielectric and Piezoelectric Ceramics, Okinawa, Japan, 1999 (inpress).
[33] A. N. Soukhojak, Y. M. Chiang, Proceedings of the 2000,12th IEEE International symposium on Applications of ferroelectrics[IEEE Catalog Number 00CH37076(ISBN0-7803-5940-2-) (2001), 557.
[34] S. A. Sheets, A. N. Soukhojak, Naoki Ohashi, Y. M. Chiang, Journal of Applied Physics **90**(10), 5287 (2001).
[35] S. E. Park, K. S. Hong, J. Appl. Phys. **79,** 383 (1996).
[36] Z. Chen, Anze ShuI, Zhenya Lu, Pingan LIU, Jour. ceramic society of Japan **114**(10), 857 (2006).
[37] N. Aparna, T. Bhimashankaram, G. S. Kumar, G. Prasad, Modern Physics Letters B **16**(26), 1007 (2002).
[38] G. K. Williamson, W. H. Hall, Acta Met. **1,** 22 (1953).
[39] S. Yamanaka, K. Kurosaki, T. Oyama, H. Muta, M. Uno,T. Matsuda, S. I. Kobayashi, J. Am. Ceram. Soc. **88**(6), 1496 (2005).
[40] G. A. Smolenskii.,V. A. Isupov, A. I. Agranovskaya, N. N. Krainik, Sov. Phys. Solid. State **2,** 2651 (1961).
[41] H. T. Martirena, J. C. Burfoot, Ferroelectric **7**, 151 (1974).
[42] G. A. Smolensky, A. I .Agranovskaja, Zh. Tech. Fiz. **28**, 1491 (1958).
[43] Chang Rong Zhou, Xin Yu Li, J. Bull Mater Scie. **30**(6), 2007.
[44] K. Uchino, S. Nomura, Ferroelectr. Lett. **44**, 55 (1982).
[45] R. Pantou, C. Dubourdieu, F. Wiess, J. Kreisel, G. Kobernik, W. Haessler, Mater. Sci. Semicond Process **5**, 237 (2003).
[46] Y. Guo, Kakimoto, H. Ohsato, Solid state Commun. **129**, 274 (2004).
[47] W. Kleemann, Int. J. Mod. Phys. **B7**, 2469 (1993).
[48] S. Prasad , K. Prasad , S. N. Choudary, T. P. Sinha, Journal of Physica **B364,** 206 (2005).
[49] T. Badapanda, S. K. Rout , S. Panigrahi, T. P. Sinha, Current Applied Physics **9**, 727 (2009).
[50] A. K. Jonscher, Philos. Mag. B. **38,** 587 (1978).
[51] Z. Lu, J. P. Bonnet, J. Ravez, P. Hagenmuller, Solid State Ionics **57,** 235 (1992).
[52] A. K. Jonscher, Dielectric Relaxation in Solids,

Chelsea Press London, 1983.
[53] R. M. Hill, C. Pickup, J. Mater. Sci. **20,** 4431 (1985).
[54] T. A .Nealon, Ferroelectric **76**, 377 (1987).
[55] Jin-Soo Kim,Jung –Won Cha, Chung Sik Kim, Jung-Nam Kim, Journal of Korean Physical Society **29**(3), 365 (1996).
[56] C. K. Suman , K. Prasad, R. N. P Choudary, Adv. Appl. Ceram. **104,** 294 (2005).
[57] C. L. Fan, D. Ciardullo,W. Huebrier, Mater. Sci. Eng. **B1009**, 1 (2003).
[58] J. E. Bauerle, J. Phys. Chem. Solids **30**, 2657 (1969).
[59] K. S. Cole, R. H. Cole, J. Chem. Phys. **9**, 341 (1941).
[60] M. A. L. Nobre, S. L. Fredi, Mater . Lett. **50**, 322 (2001).
[61] M. A. L. Nobre, S. L.Fredi, J. Phys. Chem Solids **62**, 1999 (2001).
[62] M. A. L. Nobre, S. L. Fredi, Matter. Lett. **47**, 362 (2001).
[63] R. M. Hill, A. K. Jonscher, Journal of Non-Crystalline solids **32**, 53 (1979).
[64] S. Selvasekarapandian, M. Vijayakumar, Mater. Chem. Phys., 8029, 2003.
[65] M. Pollack, T. H. Geable, Phys. Rev. **22**, 1742 (1961).
[66] G. E. Pike, Phys. Rev B6, 1571 (1972).
[67] Y. Xu, Ferroelectric Materials and Their Applications (Elsevier Science, The Netherlands, 991).
[68] O. Pérez Martínez, Ph. D. Thesis, Physics Faculty, Havana University, Cuba, 2001.
[69] A. Peláiz-Barranco, Scr. Mater. **54**, 47 (2006).

*Corresponding author: konapala@sifymail.com